High-frequency nonlinear internal waves in the Kuroshio observed by acoustic observations

Senjyu, Tomoharu
Research Institute for Applied Mechanics, Kyushu University

Endoh, Takahiro
Research Institute for Applied Mechanics, Kyushu University

Tsutsumi, Eisuke
Research Institute for Applied Mechanics, Kyushu University

Matsuno, Takeshi
Research Institute for Applied Mechanics, Kyushu University

他

出版情報：Progress in Oceanography. 237, pp.103536-, 2025-09. Elsevier
バージョン：

Progress in Oceanography 237 (2025) 103536

Contents lists available at ScienceDirect

Progress in Oceanography

journal homepage: www.elsevier.com/locate/pocean

High-frequency nonlinear internal waves in the Kuroshio observed by acoustic observations☆

Tomoharu Senjyu[a,*], Takahiro Endoh[a], Eisuke Tsutsumi[a,b], Takeshi Matsuno[a], Hirohiko Nakamura[b], Ayako Nishina[b]

[a] Research Institute for Applied Mechanics, Kyushu University, 6-1 Kasuga-koen, Kasuga City, Fukuoka 816-8580, Japan
[b] Faculty of Fisheries, Kagoshima University, 4-50-20 Shimoarata, Kagoshima City, Kagoshima 890-0056, Japan

ARTICLE INFO

Keywords:
High-frequency variation
Nonlinear internal waves
Second mode internal waves
Moored ADCP observations
Kuroshio current
Tidal currents
Seamounts

ABSTRACT

High-frequency current fluctuations in the Kuroshio current were observed using a long-range Acoustic Doppler Current Profiler (ADCP) moored in the Tokara Strait. The fluctuations were separated as deviations from the 60-min running averaged currents. The duration of individual fluctuation was 3–5 min and the active fluctuation events occurred diurnally during the period of strong Kuroshio current, suggesting both influences from the Kuroshio and tidal currents. The statistical analyses revealed that the current fluctuations were confined in the mid-depths (158–262 m) and the westward component was dominant in the eastward-flowing Kuroshio currents. Close examination of a fluctuation event revealed that strong westward and downward currents occurred in a rank-ordered wave train consisted of 3–4 waves with a period ~ 3 min. As this wave period was shorter than the ambient buoyancy period (8–13 min), the observed wave train was considered to be a packet of solitary waves (nonlinear internal waves; NLIWs). The observed current structure with a maximum amplitude at the mid-depths were similar to that of the second mode (mode-2) internal waves based on the observed stratification. In addition, the wave propagation direction estimated from the signal time lags between the ADCP transducers agreed well with the maximum current direction at mid-depths in the event. This strongly suggests that the observed current fluctuations were convex type mode-2 NLIWs. Although the NLIW generation was unclear, a role of small seamounts east of the mooring site was suggested.

1. Introduction

The Kuroshio current, a western boundary current in the North Pacific, is one of the strongest currents globally. Although the energy dissipation process in the Kuroshio is important for establishing a quasi-steady western boundary current (Wunsch, 1998, Munk and Wunsch, 1998), direct current observations in the Kuroshio using traditional mooring lines have been difficult because of vigorous currents and sharp vertical shear (Takematsu et al., 1986). However, the recent development of a long-range (>500 m) acoustic Doppler current profiler (ADCP) has enabled us to observe the detailed current structure in the Kuroshio with high temporal resolution. As the measurable distance of ADCP increases with decreasing acoustic frequency, nominally 75 kHz instruments are commonly used for long-range observations. However, trading-off for the long measurable distance, spatial and temporal resolutions become lower. Nevertheless, long-range ADCP observations are quite useful, especially in strong current regions, because we can observe the current field remotely by installing the instrument below the energetic currents.

In this study, we discussed high-frequency (3–5 min period) nonlinear internal waves (NLIWs) in the Kuroshio discovered in the Tokara Strait south of Kyushu, Japan (Fig. 1). These waves likely contribute to the energy dissipation of the Kuroshio because they accompany comparably strong counter currents that are often sufficient to reverse the Kuroshio current. This phenomenon is undiscoverable without long-range ADCP mooring, although mooring line observations with single-point current meters have revealed short-period (a few tens of minutes) current fluctuations accompanied by internal waves on the shelf break in the East China Sea (Maeda, 1979, Matsuno et al., 1997, Han et al., 2001).

The Tokara Strait is the way out of the Kuroshio from the East China Sea to the western North Pacific (Fig. 1a). In addition, the Tokara Strait

☆ This article is part of a special issue entitled: 'AMS-West Pac. and changes' published in Progress in Oceanography.

* Corresponding author.
E-mail address: senjyu@riam.kyushu-u.ac.jp (T. Senjyu).

https://doi.org/10.1016/j.pocean.2025.103536

Available online 11 July 2025

is a site of active internal tide generation because of the steep continental slope along the Ryukyu Island chain and barotropic tidal currents from the North Pacific (Niwa and Hibiya, 2011, Zhu et al., 2017, Chen et al., 2022). The interaction between the Kuroshio and internal tides on rough bottom topography induces strong turbulent mixing, which is an energy dissipation mechanism of the Kuroshio (Tsutsumi et al., 2017, Hasegawa et al., 2021, Nagai et al., 2021, Takahashi et al., 2024, Inoue et al., 2024). Furthermore, the interaction of internal tides with the Kuroshio promotes upstream internal wave energy flux through active NLIW generation owing to strong nonlinear effects (Masunaga et al., 2019). Actually, NLIWs have been observed in the northern East China Sea apart from a shelf break of more than 200 km (Lee et al., 2006),

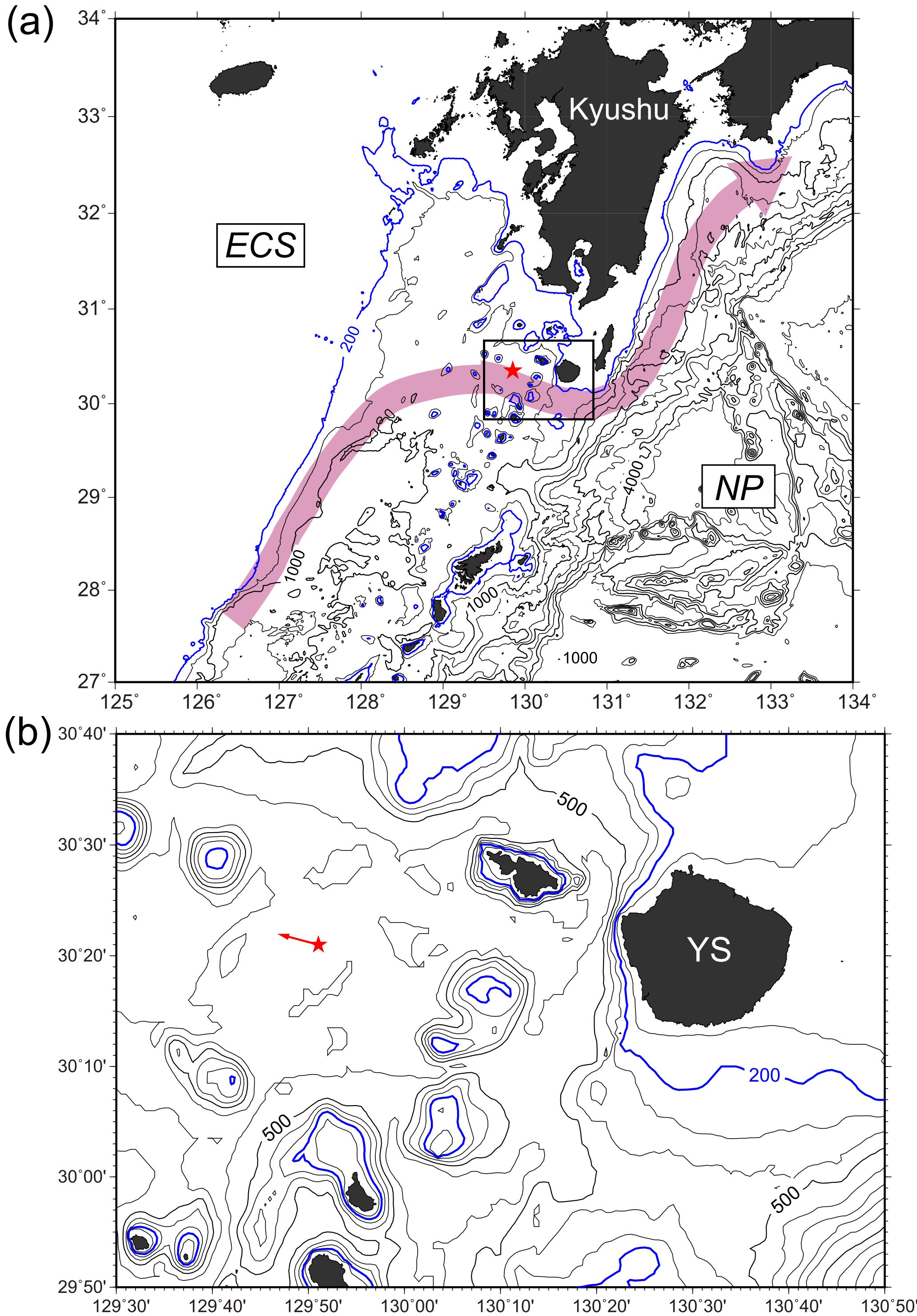

Fig. 1. Map of the observation site. (a) Bottom topography in the Tokara Strait. The red star indicates the mooring site. The contour interval is 500 m, except for the 200 m isobath, which is colored blue. ECS and NP denote the East China Sea and North Pacific, respectively. A schematic view of the Kuroshio flow path is shown by the pink winding arrow. (b) Enlarged map of the rectangular area in (a). The contour interval is 100 m, and the 200 m isobaths are depicted in blue. The NLIW propagation direction at the mooring site (red star) is indicated by the red arrow. YS denotes Yaku-shima Island. These maps were drawn using the Generic Mapping Tools version 5.4.3 (https://www.generic-mapping-tools.org/).

although their generation areas are unclear. As NLIWs contribute to oceanic mixing during dissipation (Apel, 2002), understanding their characteristics and dynamics is important when considering energy and materials budgets in the East China Sea. In addition, the Tokara Strait was recently chosen as the experimental site for Kuroshio current power generation (Shimizu et al., 2018). The NLIWs accompanying strong counter currents are likely dangerous factors that could damage the power generation system. Therefore, studies on NLIWs in this region are also needed from a marine engineering perspective.

The aim of this study is to describe the newly discovered high-frequency NLIWs in the Tokara Strait and discuss the wave structure and occurrence based on the field observation datasets. The next section explains our observations with a long-range ADCP mooring in the Kuroshio current, along with hydrographic observations. In section 3, short-period current fluctuations in the Kuroshio current are statistically investigated. In addition, detailed current structure in a typical fluctuation event is shown. The wave propagation and modal structure are discussed in section 4, along with the NLIW occurrence in relation to the background current condition. Finally, our conclusion is provided in section 5.

2. Observations

Observations in the Tokara Strait were conducted during November 15–21, 2015, using the T/V Kagoshima Maru of Kagoshima University. A long-range ADCP (Workhouse Long Ranger; 76.8 kHz, Teledyne Marine) was deployed at 30° 21.0′N, 129° 51.0′E, west of Yaku-shima Island (Fig. 1). The upward-looking ADCP was installed at a depth of 591 m (Fig. 2a). As the current speeds at this level were lower than those in the upper layers of the Kuroshio, the pitch and roll angles of the instrument were less than 0.7° and 2.0°, respectively, throughout the observation period. The range of the ADCP measurements was ~ 500 m, and the first bin range from the instrument was 16.7 m. Therefore, current measurements at depths ranging from 62 to 574 m, ~80 % of the total water column length of 648 m, were obtained at spatial and temporal intervals of 8 m and 1 min, respectively. Each current measurement was an ensemble mean for 27 pings at 2.22 s intervals, which resulted in a standard deviation of 2.81 cm s^{-1} in both horizontal and vertical components.

Temperature and salinity observations using moored instruments were not conducted because of the difficulty of obtaining mooring line observations in the Kuroshio current. Alternatively, hydrographic observations using a conductivity–temperature–depth profiler (CTD, SBE911plus, Sea Bird Electronics) were performed nearby the mooring site at ~ 2h intervals during the period from 07:30 on November 20 to 07:30 on November 21, 2015. In this study, temperature and salinity profiles measured at 07:30 on November 20, immediately after a strong counter current event, were analyzed.

3. Results

The mooring site was located in the Kuroshio during the observations (Tsutsumi et al., 2017). The time–depth diagrams of the low-pass filtered zonal and meridional currents, using the 60-min running average, were shown in Fig. 3a and 3b, respectively. The upper 300 m of the mooring site was dominated by strong east-southeastward Kuroshio currents, particularly beginning in the afternoon of November 17, along with semidiurnal tidal fluctuations. The deviations from the low-pass filtered zonal and meridional currents (referred to u' and v', respectively) with considerable amplitude (>15 cm s^{-1}) were superimposed in Fig. 3. These short-period (<60 min) current fluctuations appeared to occur frequently at depths of 150–300 m. Fig. 4 shows the time series of u' and v' for the period 12:00–15:00 on November 18, 2015. Notable current fluctuations sporadically occurred in the depth range 182–262 m, showing several active fluctuation periods (events) of 12:50–13:10, 13:30–14:10, and 14:40–15:00. Duration of individual fluctuation in the events was typically 3–5 min.

The vertical profiles of the integrated u' and v' amplitudes for the observation period showed values > 200 cm s^{-1} in the depth range 158–262 m (the core layer), showing a maximum value in the profiles (Fig. 5a). The directional distribution of the short-period current fluctuations in the core layer indicates that the westward currents were dominant for the observation period (Fig. 5b). The largest integrated fluctuations were southwestward (6288.6 cm s^{-1}); however, the northwestward (5961.7 cm s^{-1}) and north-northwestward (5607.3 cm s^{-1}) fluctuations—the second and third largest components, respectively—occupied 18.6 % of the total fluctuations (62044.9 cm s^{-1}). In addition, the short-period current fluctuations occurred diurnally from November 17–21 (Fig. 6a and 6b), in which the background Kuroshio current was strong (Fig. 3). This suggests both influences from the Kuroshio and tidal currents.

As a typical example, an event during 07:12–07:26 on November 20, 2015, was closely investigated because a CTD observation was performed immediately after the strong current fluctuations. The temporal

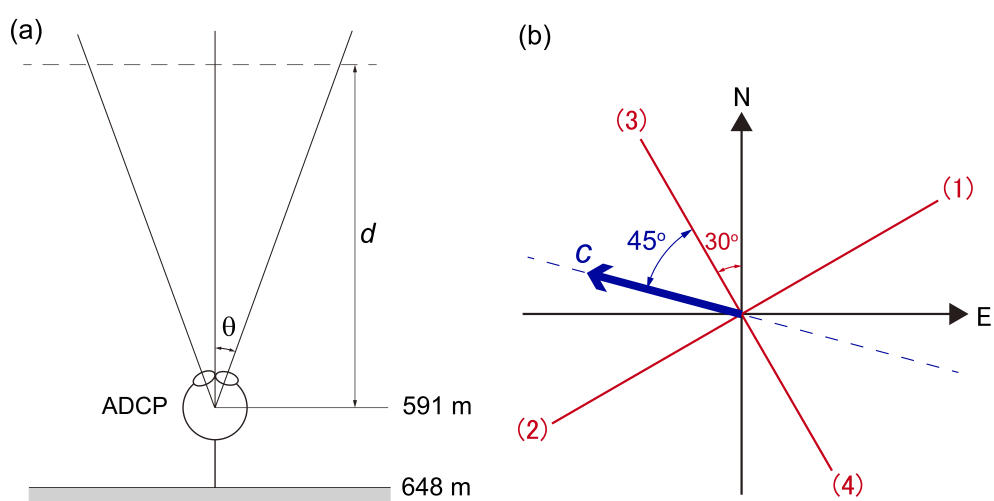

Fig. 2. (a) Design of the ADCP mooring. The ADCP was installed upward-looking at a depth of 591 m above the seabed at 648 m. Oblique lines from the ADCP indicate sound beams from the two opposite transducers directed to angle θ from the vertical. The distance between the instrument and the target depth indicated by the horizontal broken line is d. (b) The NLIW propagation direction (blue arrow labeled c) in Earth (black) and ADCP (red) coordinates. N and E denote the north and east directions, respectively, in Earth coordinates. The numbers in parentheses indicate the transducer number in the ADCP coordinates.

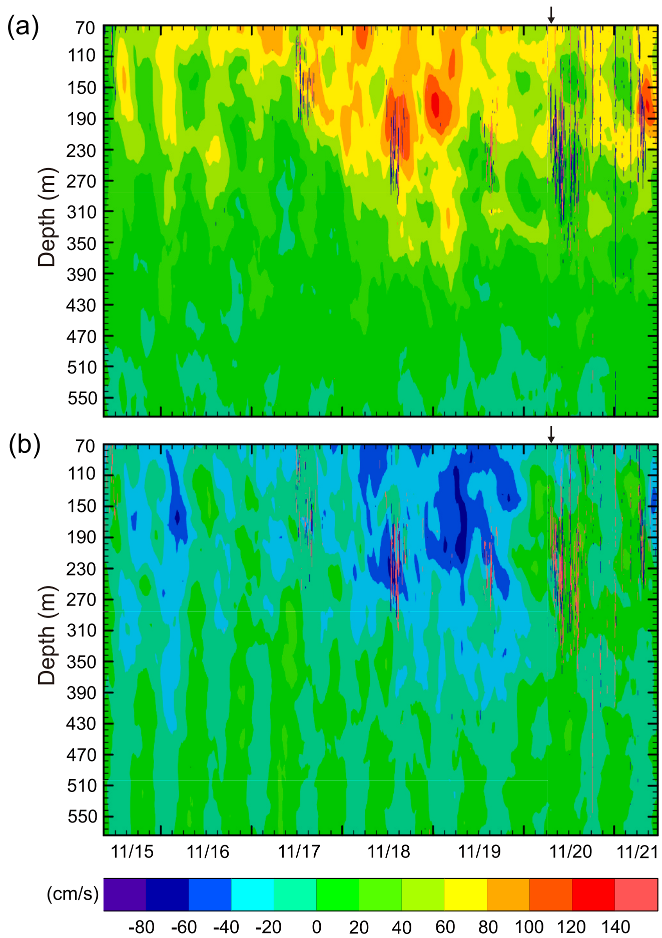

Fig. 3. Time–depth diagrams for the low-pass filtered current field with a 60-min moving average: (a) zonal and (b) meridional components. Short-period (<60 min) current fluctuations with amplitudes >15 cm s^{-1} are superimposed (red: positive, blue: negative). Arrow at the upper margin of each panel indicates the event in Fig. 8.

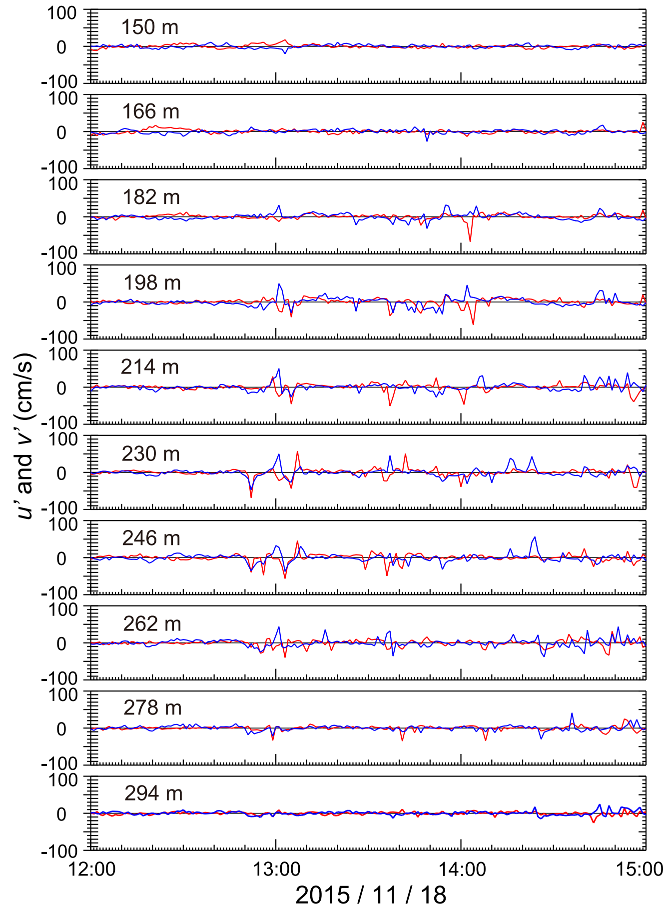

Fig. 4. Time series of u' (red) and v' (blue) at representative depths from 150–294 m during the period of 12:00–15:00 on November 18, 2015.

evolution of the zonal (u), meridional (v), and vertical (w) velocity profiles exhibited considerable fluctuations at approximately 200 m, whereas stable profiles were observed below 300 m and above 120 m throughout the period, indicating a vertical scale of disturbance of ~ 150 m (Fig. 7). Just before the event at 07:12, the zonal currents at 200 m were approximately 60 cm s^{-1}, reflecting the Kuroshio (Fig. 7a). However, the currents from 150–200 m weakened gradually beginning at 07:13 and reversed direction at 07:15. A maximum westward current (−28.1 cm s^{-1}) was recorded at 07:16 at 190 m. After resuming to approximately 60 cm s^{-1} at 07:17, the next current reversal (−23.6 cm s^{-1}) occurred at 182 m at 07:18 (Fig. 7b). A sudden current reversal occurred again at 07:21 accompanying the maximum current speed (−51.4 cm s^{-1}) at 198 m; the current resumed to approximately 60 cm s^{-1} at 07:20. Extremely strong downward currents (>10 cm s^{-1}) were observed at the same depths during the zonal flow reversals (Fig. 7g–i). The meridional currents also showed northward fluctuations at depths of 155–220 m during the westward currents (Fig. 7d–f).

The three zonal current reversals at 07:16, 07:18, and 07:21 are clearly depicted in the time–depth diagram for u at depths of 150–230 m and were accompanied by strong downward currents (Fig. 8a and 8c). Corresponding northward currents > 30 cm s^{-1} appeared in v, although a second signal occurred at 07:19 (Fig. 8b). The weaker signals in u and w at 07:25 at 182 m are likely part of the wave train, suggesting a rank ordered wave train. Assuming that the wave train consisted of four waves with a duration of 12 min (from 07:13 to 07:25), the wave period during the event was approximately 3 min. However, the CTD observations immediately after the event (conducted during 07:22–07:34) revealed that this wave period was too short compared with the buoyancy period (8–13 min) at depths of 150–200 m (Fig. 9a). The CTD station (30° 20.1′N, 129° 52.4′E) was 2.7 km apart from the mooring site; however, the assumption that the basic stratification at the mooring site was almost same as that at the CTD station is reasonable. This suggests that the observed wave train was a packet of solitary waves (NLIWs) with an individual amplitude, wavelength, and phase velocity for each wave.

A relatively weak echo intensity layer existed between the strong echo intensities (>90 counts) above 134 m and below 246 m (Fig. 8d). The upper strong echo intensities were associated with a sharp pycnocline (Fig. 9a). On the other hand, the lower strong echo intensities were likely a sound scattering layer due to descending plankton because they were part of the vertically-migrating strong echoes descending in morning and ascending in evening (Fig. 10). In the intermediate weak-echo intensity layer, remarkable echoes (80–90 counts) occurred at depths of 214–238 m below the wave train between 07:12 and 07:30. In particular, considerable echo intensity events (85–90 counts) occurred at 07:16–07:19, 07:20–07:21, 07:23–07:25, and 07:28, suggesting a relationship to the wave train.

4. Discussion

We discuss the propagation of NLIWs observed during 07:12–07:26 on November 20, 2015 (Figs. 7 and 8). Endoh et al. (2022) demonstrated that direction and speed of NLIW propagation can be estimated from a single moored-ADCP by close examination of the phase relationships among the echo signals. The estimation procedure was described in

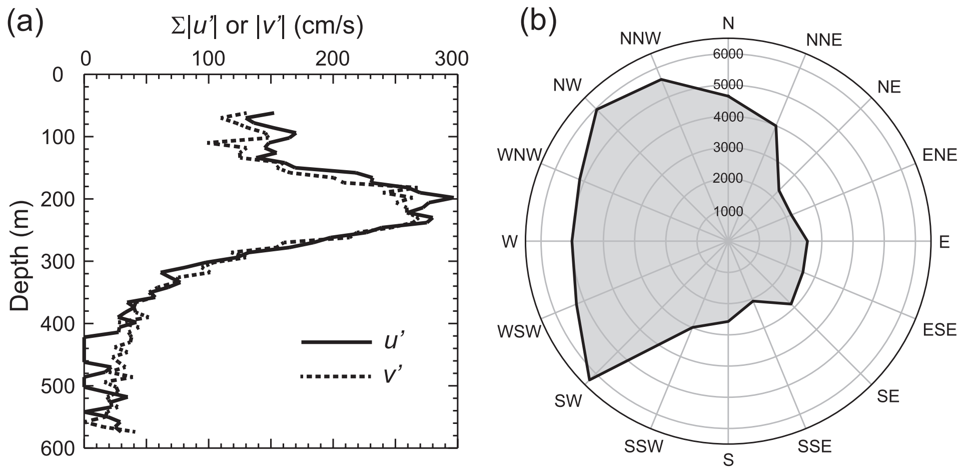

Fig. 5. (a) Profiles of the integrated u' (solid line) and v' (broken line) amplitudes >15 cm s^{-1} for the observation period. (b) Directional distribution of u' and v' with amplitudes >15 cm s^{-1} integrated for the observation period.

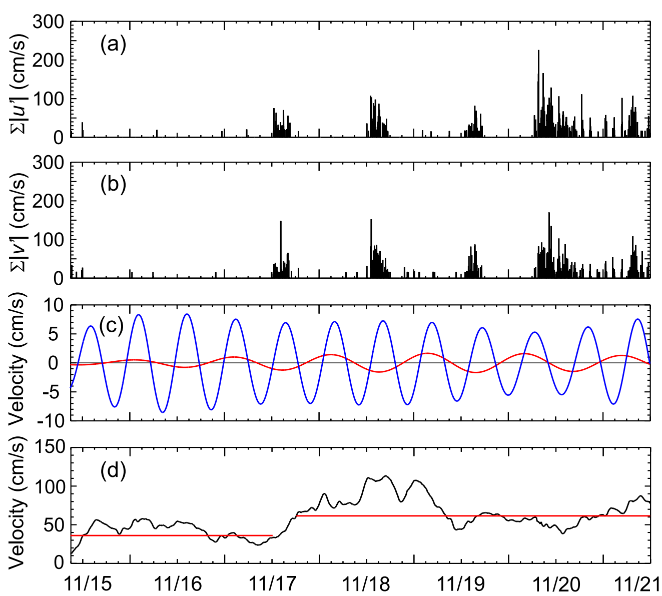

Fig. 6. Time series of vertically integrated u' (a) and v' (b) for the core layer (158–262 m). (d) Vertically averaged zonal velocities for the core layer in which the diurnal (red) and semidiurnal (blue) barotropic flows shown in (c) were subtracted. The two red lines in (d) indicate the mean velocities for the weak and strong background current periods.

Appendix A. Appling the procedure to the counter current event, the wave propagation was estimated to be 285° in direction and 119 cm s^{-1} in magnitude. This direction is shown by the red arrow in Fig. 1b. Although the mooring site was located on a relatively flat bottom approximately 100 km from the continental slope, there were several seamounts on the opposite side of the wave propagation. The summit depth of the seamounts is ~ 200 m, which coincides with the core layer (158–262 m) of current fluctuations. This implies that the small-scale (10–20 km) seamounts in the Tokara Strait play a role in NLIW generation. The considerable influences of bumpy topography (seamounts) on NLIW formation and evolution are reported from continental slope and shelf regions in the northern South China Sea (Xie et al, 2019). The horizontal wave scale can be estimated from the wave propagation speed and the duration of wave passing, although the ADCP measurement interval (1 min) was insufficient to resolve the detailed waveform. If we regarded the duration of counter currents of 1–2 min as the time required for a wave to pass the mooring site (Fig. 8), the horizontal wave scale was 71–143 m, which agrees with that of the NLIWs on the East China Sea shelf (~100 m) (Endoh et al., 2022).

As NLIWs generally disintegrate from linear internal waves due to nonlinear effects (Apel, 2002; Rayson et al., 2019), we assumed that the observed NLIWs retained the vertical structure of the original linear internal waves. The modal current structure at the mooring site can be calculated by solving the equation,

$$\frac{d^2W}{dz^2} + \kappa^2\frac{N^2 - \omega^2}{\omega^2 - f^2}W = 0 \qquad (1)$$

where W is the vertical structure function, N is the buoyancy frequency based on the observed density stratification (Fig. 9a), ω is the wave frequency, f is the inertial frequency (0.73×10^{-4} s^{-1} at 30°N), and κ is the horizontal wave number (Cushman-Roisin and Beckers, 2011). However, it should be noted that the internal tide with the K_1 period (23.93 h) was absent at the mooring site because the K_1 period is longer than the inertial period at this latitude (23.69 h), although short-period current fluctuations occurred diurnally. Therefore, nonhydrostatic internal waves which were generated at the seamounts on the opposite side of the wave propagation were assumed (Fig. 1b). In this case, the wave frequency is determined as eigenvalue problem of Eq. (1) because the vertical structure function depends on the wave frequency. The horizontal wavelength of the internal wave was assumed to be 10 km ($\kappa = 6.28 \times 10^{-4}$ m^{-1}) according to the horizontal dimension of the seamounts. The horizontal current profiles for the leading three modes indicate that the observed current structure corresponds to the second mode (mode-2) internal waves with a maximum amplitude at ~ 200 m (Fig. 9b). Actually, the density profile immediately after the counter current event showed a three-layer structure with a middle layer of 150–330 m (Fig. 9a), which is favorable for the generation of convex type mode-2 NLIW which has a bulge-shaped middle layer in a three-layer ocean model (Yang et al., 2010). A typical character of the convex type mode-2 NLIW is that the wave propagates same direction as the current in the middle layer (Yang et al., 2009, 2010; Ramp et al., 2015). The direction and speed at the maximum counter current during the event (07:21 at 198 m) were 280.2° and 52.2 cm s^{-1}, respectively (Fig. 7). The estimated wave propagation direction (285°) coincided with the maximum counter current direction. This strongly suggests that the observed current fluctuations were mode-2 NLIWs. Considering the predominance of westward current fluctuations in the core layer (Fig. 5), most of the short-period current fluctuations were likely due to westward-propagating mode-2 NLIWs.

To demonstrate the bulge-shaped mode-2 NLIW, we tried to estimate the vertical isopycnal displacements (h) due to vertical advection from successive time integrations of the vertical velocities at a time step of 1

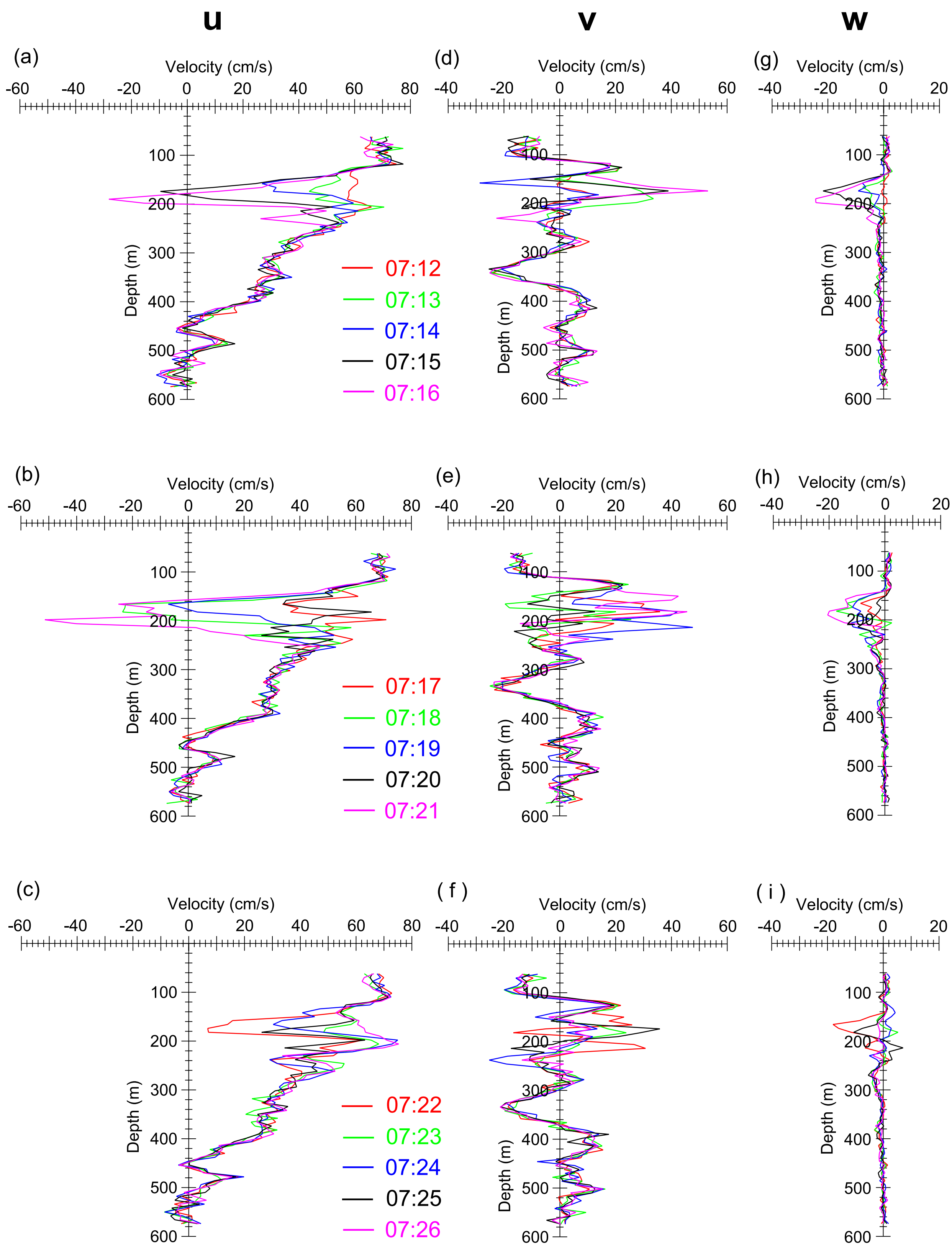

Fig. 7. Vertical profiles of *u* (left), *v* (center), and *w* (right) for periods 07:12–07:16 (a, d, g), 07:17–07:21 (b, e, h), and 07:22–07:26 (c, f, i).

min:

$$h = \int w dt \tag{2}$$

The contours in Fig. 8d show the temporal evolution of the isopycnals, which were placed at each observation depth at 07:10. Note that the contours do not show an even density interval, namely, not in a uniform density stratification at the initial time. The isopycnals at depths of 166–190 m abruptly depressed beginning at 07:15 owing to strong downward currents (Fig. 8c) and converged into a layer at 206–230 m.

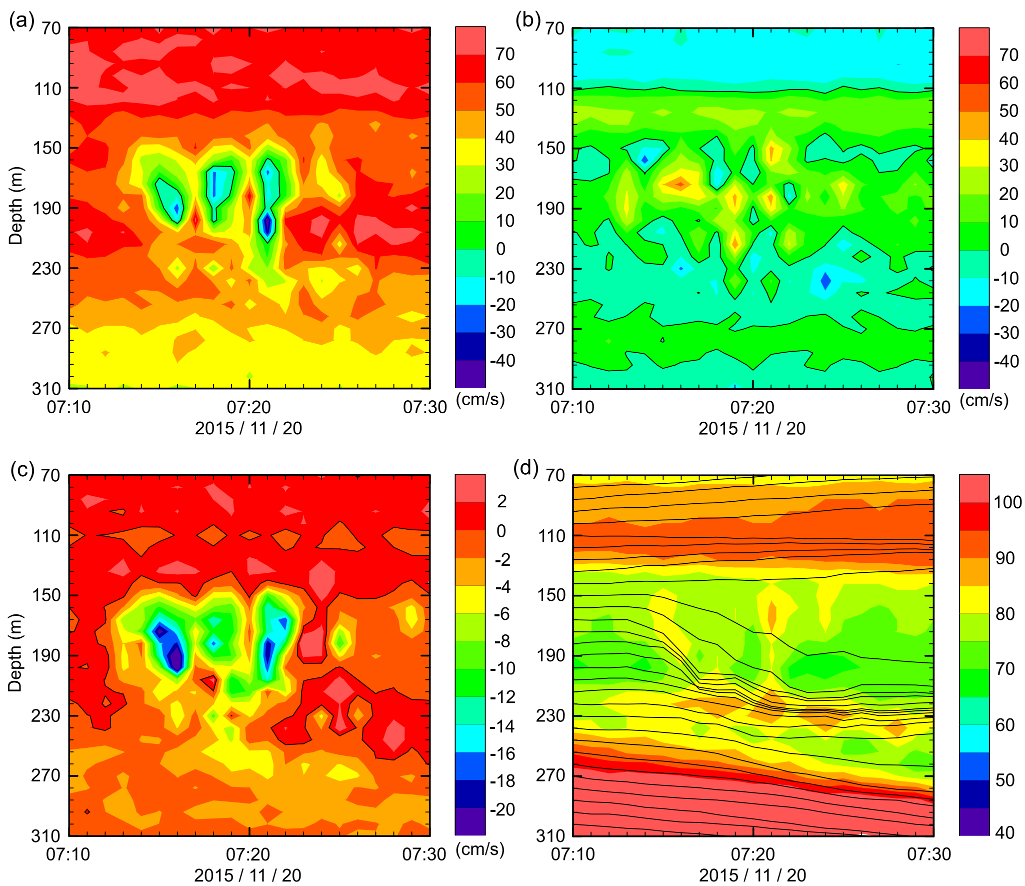

Fig. 8. Time–depth diagrams for the period of 07:10–07:30 on November 20, 2015. (a) *u*, (b) *v*, (c) *w*, and (d) echo intensity (color). The unit of echo intensity is counts. The contours in (d) indicate the estimated displacement of isopycnals placed at observation depths at 07:10. The contours in (a), (b), and (c) indicate zero line.

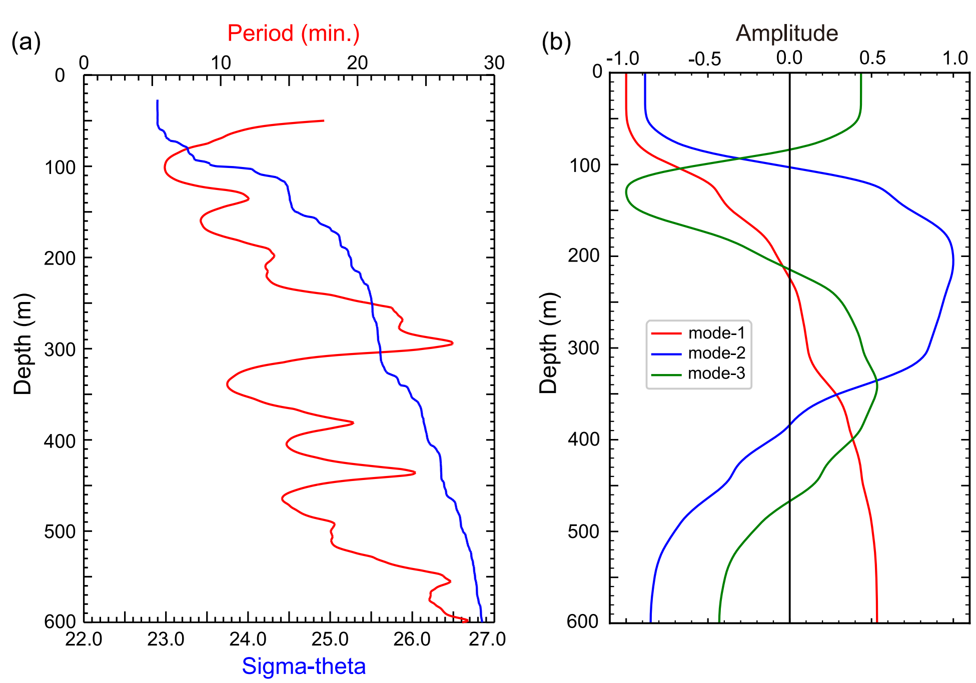

Fig. 9. (a) Vertical profiles of potential density (blue) and buoyancy period (red) nearby the mooring site immediately after the counter current event (07:22–07:34). (b) Horizontal current profiles of the leading three normal modes at the mooring site. Each profile is normalized by the maximum amplitude in each mode.

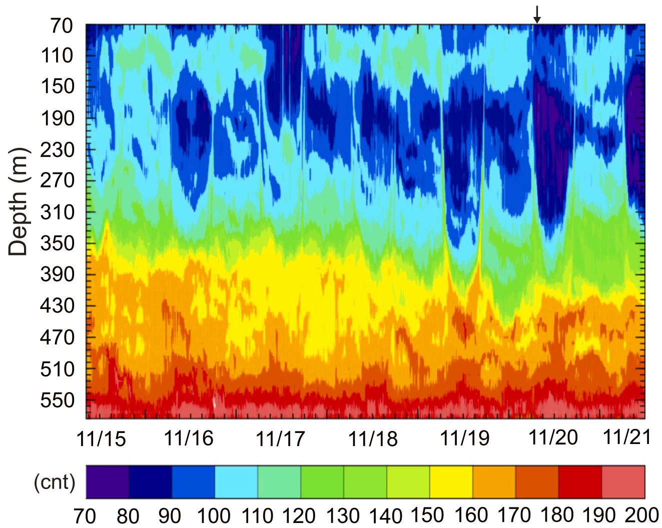

Fig. 10. Time–depth diagram of echo intensity for the observation period. Arrow at the upper margin indicates the event in Fig. 8.

The closed contours coincided with strong echo intensities below the wave train. This suggests that the strong echo intensities were attributed to the steep density gradient produced by the strong downward currents. Although relatively strong echo intensities occurred above the wave train (142–174 m) at 07:14–07:16, 07:20–07:22, and 07:24, bulge-shaped density contours were not calculated. This is probably owing to insufficient temporal resolution in the vertical velocity measurements. In addition, as the waves propagated against the Kuroshio current, considerable distortions may occur in the waveform.

To investigate the relationship to the Kuroshio and tidal currents, firstly, the tidal components were extracted from the zonal currents using two separate 6th-order Butterworth band-pass filters, one for semidiurnal (10–14 h) and one for diurnal (22–26 h) components. The vertically averaged currents in both bands were regarded as barotropic tidal currents (Fig. 6c). The amplitude of the diurnal currents was less than one-third that of the semidiurnal currents; however, NLIWs appeared to occur when the westward diurnal current peaked during the second half of the observation period, during which the diurnal current amplitude increased. Next, by subtracting the barotropic diurnal and semidiurnal currents from the low-pass filtered u, the background zonal currents were estimated. The vertically averaged background currents for the core layer were positive throughout the observation period, reflecting the Kuroshio current (Fig. 6d). Although the baroclinic semidiurnal internal tides were superimposed on the currents, the observation period can be divided into two periods based on the background current speed: the relatively weak current period from the beginning of the observation (08:53 on November 15) to 12:00 on November 17 and the strong current period due to the Kuroshio from 18:00 on November 17 to the end of the observation (11:29 on November 21). The mean current speeds for the former and latter periods were 36.0 and 61.5 cm s^{-1}, respectively. The period of active NLIWs coincided with the strong background current period. This indicates that NLIWs were activated when the background Kuroshio current was strong and the diurnal tidal current was westward, without relationship to the semidiurnal tidal current. However, the mechanism for this variation is unclear. Ramp et al. (2012) discussed the diurnal appearance of mode-2 NLIWs in Luzon Strait based on the internal Froude number ($Fr = U/c_i$), where U and c_i denote the speeds of the background current and the i-th mode internal wave, respectively. The key of their explanation is that the dominant diurnal tidal currents modulate the background current U. However, in this study, the amplitude of semidiurnal currents was larger than that of diurnal currents throughout the observation period, which cannot explain the diurnal appearance of NLIWs. A possibility is the earth rotation effect which suppresses the NLIW formation through the dispersion effect. Farmer et al (2009) explained the diurnally modulated mode-1 NLIWs in the semidiurnal currents by this mechanism. To elucidate this mystery, further studies are needed.

5. Conclusion

We concluded that high-frequency current fluctuations in the Kuroshio current observed by the long-range ADCP observations were mode-2 NLIWs, although the generation of NLIWs could not be elucidated in this study. The aim of this study was to describe the structure and occurrence of the current fluctuations, because this is the first repot of mode-2 NLIW in the Tokara Strait. The statistical analysis revealed that the current fluctuations were confined in the mid-depths (158–262 m) and the westward component was dominant in the eastward-flowing background Kuroshio currents. The typical duration of individual fluctuation was 3–5 min. In addition, the active current fluctuation events occurred diurnally during the period of strong Kuroshio current, suggesting both influences from the Kuroshio and tidal currents. Close examination of the fluctuation event during 07:12–07:26 on November 20, 2015 revealed that strong westward and downward currents occurred in a rank-ordered wave train consisted of 3–4 waves with a period ~ 3 min. The wave propagation direction and speed were estimated to be 285°and 119 cm s^{-1}, respectively, from signal time lags between the ADCP transducers. This direction agreed with the maximum current direction at mid-depths, which is a typical character of convex type mode-2 NLIW in a 3-layer oceanic model. The horizontal wave scale was estimated to be 71–143 m assuming the propagation speed. Small seamounts east of the mooring site were suggested to play a role in NLIW generation.

Mode-2 NLIW has generally much shorter lifetime (~few hours) than that of mode-1 NLIW (~few days), which suggests that mode-2 NLIW is an agent of local energy dissipation (Shroyer et al., 2010). The energy and lifetime of mode-2 NLIWs in the Tokara Strait are unknown; however, considering that the Kuroshio always passes through the strait where many small-scale seamounts exist, the NLIW generation in the Tokara Strait could be a major energy dissipation mechanism in the Kuroshio dynamical system, similar to the Izu-Ogasawara ridge south of Japan (Masunaga et al., 2019). To confirm role of the Tokara Strait, long-period mooring observations at several points using acoustic instruments such as long-range ADCPs and inverted echo sounders are desired, as are frequent satellite observations and numerical model studies reproducing a realistic Kuroshio current on the detailed bottom topography.

Data availability

The datasets used in this study were deposited in the Kyushu University Institutional Repository (QIR) as doi:10.48708/7159627.

CRediT authorship contribution statement

Tomoharu Senjyu: Writing – original draft, Resources, Formal analysis, Conceptualization, Writing – review & editing, Visualization, Investigation, Data curation. **Takahiro Endoh:** Software, Formal analysis, Methodology. **Eisuke Tsutsumi:** Investigation, Formal analysis. **Takeshi Matsuno:** Project administration, Funding acquisition, Investigation, Formal analysis. **Hirohiko Nakamura:** Validation, Project administration, Resources, Investigation. **Ayako Nishina:** Validation, Investigation, Resources, Data curation.

Funding

This study was supported by JSPS KAKENHI (grant number JP15H05821).

Declaration of competing interest

The authors declare that they have no known competing financial interests or personal relationships that could have appeared to influence the work reported in this paper.

Acknowledgements

The authors thank the captain and crew of the T/S Kagoshima Maru of Kagoshima University and all the participants of the KG1515 cruise. The original manuscript has been greatly improved by insightful comments from the anonymous reviewers.

Appendix A. . Estimation of NLIW propagation from the ADCP echo intensities

Our ADCP measured sound echoes from depth using sound beams emitted from four transducers arranged at right angles (transducers (1) to (4), Fig. 2b). As the beams are directed at an angle θ to the vertical, the echo signals received by each transducer originate from horizontally separated points (Fig. 2a). We usually regard the average signal from the four transducers as an echo intensity measurement. However, when the horizontal wave scale is shorter than $2d \tan \theta$, where d is the distance between the instrument and the target depth, a phase mismatch between the echo signals received by the opposing transducers induces erroneous measurements (Scotti et al., 2005). Nevertheless, close examination of the phase relationships among the echo signals can estimate direction and speed of the wave propagation (Endoh et al., 2022).

Although each transducer detected several strong signals during the event, we regarded the three signals marked by dashed blue lines as wave trains (Fig. A1). It is clear that the first signals in beams (1) and (4) (occurring at 07:15 and 07:16, respectively) led by 2–3 min to those of beams (2) and (3) (at 07:18). Accordingly, the second and third signals in beams (2) and (3) lagged those in beams (1) and (4) by 2–3 min. Therefore, we assumed the representative time lags between the opposing transducers (ΔT_{21} and ΔT_{43}) to be − 180 and 180 s, respectively. The direction of the signal propagation can be estimated by:

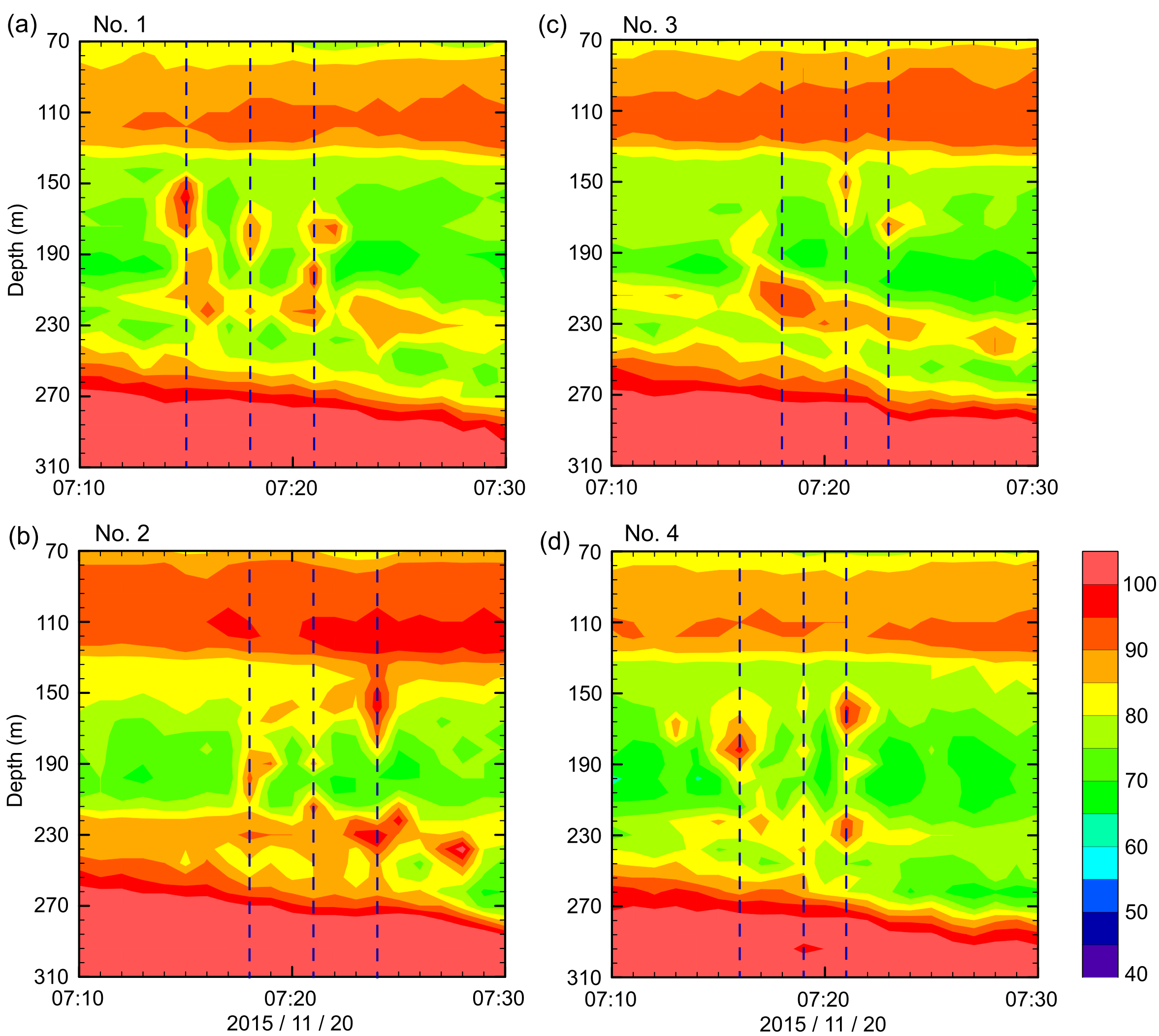

Fig. A1. Time–depth diagrams of the echo intensity from the (a) No. 1, (b) No. 2, (c) No. 3, and (d) No. 4 transducers. The dashed blue lines in each panel indicate the NLIWs.

$$\phi_{ADCP} = tan^{-1}\left(\frac{\Delta T_{43}}{\Delta T_{21}}\right) \quad \text{(A1)}$$

where ϕ_{ADCP} is measured anticlockwise from the transducer (1) axis (ADCP coordinate, Fig. 2b). In this case, $\phi_{ADCP} = \tan^{-1}(-1) = 135^\circ$ or 315°; however, considering that the signals in beams (1) and (4) led to those in beams (2) and (3), $\phi_{ADCP} = 135^\circ$ is reasonable. The propagation direction in the ADCP coordinate can be transformed to that in the Earth coordinate (ϕ), which is measured clockwise from north, by

$$\phi = 90^{\circ} - \phi_{ADCP} + \varphi_h \quad \text{(A2)}$$

where φ_h denotes the heading angle, which is the deviation of the transducer (3) axis from the north. Because the heading angle during the event was approximately 330°, the direction of the wave train propagation was estimated to be 285°.

The distance between the points where the echo signals received by the opposing transducers were emitted was 2d tan θ (Fig. 2a). If we assume a plane wave in the ADCP coordinate system, the speed of signal propagation c is:

$$c = \frac{2dtan\theta}{\Delta T_{21}} cos\phi_{ADCP} = \frac{2dtan\theta}{\Delta T_{43}} sin\phi_{ADCP} \quad \text{(A3)}$$

The transducer angle (θ) of the ADCP (Long Ranger, Teledyne Marine) was 20°. Therefore, when the target depth is 174 m (i.e., $d = 417$ m) considering the counter current depth range (Figs. 7 and 8), the wave propagation speed is estimated to be 119 cm s^{-1}.

The distance between the beams emitted from the opposing transducers (2d tan θ) at a depth of 174 m was 303.6 m. On the other hand, the estimated horizontal wave scale was 71–143 m, as discussed in section 4. This finding is consistent with the assumption that the horizontal wave scale was shorter than 2d tan θ.

References

Apel, J. R. (2002) Oceanic internal waves and solitons. An atlas of oceanic internal solitary waves. 1, 1–40.

Chen, J., Zhu, X.-H., Wang, M., Zheng, H., Zhao, R., Nakamura, H., Yamashiro, T., 2022. Incoherent signatures of internal tides in the Tokara Strait modulated by the Kuroshio. Prog. Oceanogr. 206, 102863.

Cushman-Roisin, B., Beckers, J.M., 2011. Introduction to Geophysical Fluid Dynamics: Physical and Numerical Aspects, Second ed. Academic, Massachusetts.

Endoh, T., Tsutsumi, E., Hong, C.-S., Baek, G.-N., Chang, M.-H., Yang, Y.J., Matsuno, T., Lee, J.H., 2022. Estimating propagation speed and direction, and vertical displacement of second-mode nonlinear internal waves from ADCP measurements. Cont. Shelf Res. 233. https://doi.org/10.1016/j.csr.2021.104644.

Farmer, D., Li, Q., Park, J.-H., 2009. Internal wave observations in the South China Sea: The role of rotation and non-linearity. Atmos.–Ocean 47, 267–280.

Han, I.-S., Kamio, K., Matsuno, T., Manda, A., Isobe, A., 2001. High frequency current fluctuations and cross-shelf flows around the pycnocline near the shelf break in the East China Sea. J. Oceanogr. 57, 235–249.

Hasegawa, D., Matsuno, T., Tsutsumi, E., Senjyu, T., Endoh, T., Tanaka, T., Yoshie, N., Nakamura, H., Nishina, A., 2021. How a small reef in the Kuroshio cultivates the ocean. Geophys. Res. Lett. 48. https://doi.org/10.1029/2020GL092063.

Inoue, R., Tsutsumi, E., Nakamura, H., 2024. Numerical simulation of the Kuroshio flowing over the Hirase seamount in the Tokara Strait in autumn: Tidal vortex shedding in a baroclinic jet. J. Phys. Oceanogr. 54, 153–172.

Lee, J.H., Lozovatsky, I., Jang, S.-T., Jang, C.J., Hong, C.S., Fernando, H.J.S., 2006. Episodes of nonlinear internal waves in the northern East China Sea. Geophys. Res. Lett. 33, L18601. https://doi.org/10.1029/2006GL027136.

Maeda, A., 1979. Short internal waves on the margin of the continental shelf of the East China Sea. La mer 17, 18–27.

Masunaga, E., Uchiyama, Y., Yamazaki, H., 2019. Strong internal waves generated by the interaction of the Kuroshio and tides over a shallow ridge. J. Phys. Oceanogr. 49, 2917–2934. https://doi.org/10.1175/JPO-D-18-0238.1.

Matsuno, T., Hibiya, T., Kanari, S., Kobayashi, C., 1997. Small scale internal waves and turbulent fluctuations near the continental shelf break in the East China Sea. J. Oceanogr. 53, 259–267.

Munk, W.H., Wunsch, C., 1998. Abyssal recipes II: Energetics of tidal and wind mixing. Deep-Sea Res. I 45, 1977–2010.

Nagai, T., Hasegawa, D., Tsutsumi, E., Nakamura, H., Nishina, A., Senjyu, T., Endoh, T., Matsuno, T., Inoue, R., Tandon, A., 2021. The Kuroshio flowing over seamounts and associated submesoscale flows drive 100-km-wide 100-1000-fold enhancement of turbulence. Comm. Earth & Env. 2, 170. https://doi.org/10.1038/s43247-021-00230-7.

Niwa, Y., Hibiya, T., 2011. Estimation of baroclinic tide energy available for deep ocean mixing based on three-dimensional global numerical simulations. J. Oceanogr. 67, 493–502. https://doi.org/10.1007/s10872-011-0052-1.

Ramp, S.R., Yang, Y.J., Reeder, D.B., Bahr, F.L., 2012. Observations of mode-2 nonlinear internal wave on the northern Heng-Chun Ridge south of Taiwan. J. Geophys. Res. 117, C03043. https://doi.org/10.1029/2011JC007662.

Ramp, S.R., Yang, Y.J., Reeder, D.B., Buijsman, M.C., Bahr, F.L., 2015. The evolution of mode-2 nonlinear internal waves over the northern Heng-Chun Ridge south of Taiwan. Nonlinear Process Geophys. 22, 413–431.

Rayson, M.D., Jones, N.L., Ivey, G., 2019. Observations of large-amplitude mode-2 nonlinear internal waves on the Australian North West shelf. J. Phys. Oceanogr. 40, 309–328.

Scotti, A., Butman, B., Beardsley, R.C., Alexander, P.S., Anderson, S., 2005. A modified beam-to-Earth transformation to measure short-wavelength internal waves with an acoustic Doppler current profiler. J. Atmos. Ocean Tech. 22, 583–591.

Shimizu, M., Nagaya, S., Ueno, T., Saito, H., Murata, S., Ito, A., 2018. Development and demonstration test for floating type ocean current turbine system conducted in Kuroshio Current. Grand Renew. Energy. Proceedings.

Shroyer, E.L., Moum, J.N., Nash, J.D., 2010. Mode 2 waves on the continental shelf: Ephemeral components of the nonlinear internal wavefield. J. Geophys. Res. 115, C07001. https://doi.org/10.1029/2009JC005605.

Takahashi, A., Lien, R.-C., Kunze, E., Ma, B., Nakamura, H., Nishina, A., Tsutsumi, E., Inoue, R., Nagai, T., Endoh, T., 2024. Energetic stratified turbulence generated by Kuroshio–seamount interactions in Tokara Strait. J. Phys. Oceanogr. 54, 461–484.

Takematsu, M., Kawatate, K., Koterayama, W., Suhara, T., Mitsuyasu, H., 1986. Moored instrument observations in the Kuroshio south of Kyushu. J. Oceanogr. Soc. Japan 42, 201–211.

Tsutsumi, E., Matsuno, T., Lien, R.-C., Nakamura, H., Senjyu, T., and Guo, X. (2017) Turbulent mixing within the Kuroshio in the Tokara Strait. J. Geophys. Res. Oceans, 122. doi:10.1002:2017JC013049.

Wunsch, C., 1998. The work done by the wind on the oceanic general circulation. J. Phys. Oceanogr. 28, 2332–2340.

Xie, J., He, Y., Cai, S., 2019. Bumpy topographic effects on the transbasin evolution of large-amplitude internal solitary wave in the northern South China Sea. J. Geophys. Res. Oceans 124, 4677–4695.

Yang, Y.J., Fang, Y.C., Tang, T.Y., Ramp, S., 2010. Convex and concave types of second baroclinic mode internal solitary waves. Nonlinear Process Geophys. 17, 605–614.

Yang, Y.J., Fang, Y.C., Chang, M.-H., Ramp, S.R., Kao, C.-C., Tang, T.Y., 2009. Observations of second baroclinic mode internal solitary waves on the continental slope of the northern South China Sea. J. Geophys. Res. 114, C10003. https://doi.org/10.1029/2009JC005318.

Zhu, X.-H., Nakamura, H., Dong, M., Nishina, A., Yamashiro, T., 2017. Tidal currents and Kuroshio transport variations in the Tokara Strait estimated from ferryboat ADCP data. J. Geophys. Res. Oceans 122, 2120–2142.